INTERNATIONAL JOURNAL FOR NUMERICAL METHODS IN FLUIDS
Int. J. Numer. Meth. Fluids 2004; **45**:625–642 (DOI: 10.1002/fld.716)

A compact numerical algorithm for solving the time-dependent mild slope equation

Pengzhi Lin*,†

Department of Civil Engineering, National University of Singapore, Singapore

SUMMARY

The mild slope equation has been widely used to describe combined wave refraction and diffraction. In this study, a new numerical algorithm is developed to solve the time-dependent mild slope equation in a second-order hyperbolic form. The numerical algorithm is based on a compact and explicit finite difference method that is second-order accurate in both time and space. The algorithm has the similar structure to the leap-frog method but is constructed on three time levels for the second-order time derivative term. The numerical model has the capability of simulating transient wave motion by correctly predicting the speed of wave energy propagation, which is important for the real-time forecast of the arrival time of storm waves generated in the far field. The model is validated against analytical solution for wave shoaling and experimental data for combined wave refraction and diffraction over a submerged elliptic shoal on a slope (Coastal Eng. 1982; **6**:255). Lastly, the realistic scale Homma's island (Geophys. Mag. 1950; **21**:199) is studied with the use of various wave periods of $T = 720$ s, $T = 120$ s, and $T = 24$ s. These wave periods correspond to long, intermediate, and short waves for the given topography, respectively. Comparisons are made between numerical results and existing analytical solutions in terms of the wave amplification around the island, which serves as the indicator for the potential wave runup. Excellent agreements are obtained. The model runs on a PC (Pentium IV 1.8 GHz) and the computer capacity allows the computation of a mesh system up to 3000×3000, which is equivalent to about 150×150 waves or a large area of 540 km $\times$ 540 km for a wave train with the period of $T = 60$ s.

KEY WORDS: time-dependent mild slope equation; wave refraction; wave diffraction; compact numerical algorithm; storm wave simulation; real-time wave forecast

INTRODUCTION

To simulate linear wave propagation from deep water to shallow water with the use of a unified equation model, the mild slope equation can serve as a good candidate. The mild

*Correspondence to: P. Lin, Department of Civil Engineering, National University of Singapore, Singapore.
†E-mail: cvelinpz@nus.edu.sg

Contract/grant sponsor: National University of Singapore; contract/grant number: R-264-000-121-112
Contract/grant sponsor: Meteorological Service Singapore; contract/grant number: R-264-000-121-291

Published online 8 April 2004
Received 30 May 2003
Revised 20 January 2004

slope equation, which can be derived from the potential flow theory (e.g. References [1–3]), has been widely used to describe the combined wave refraction and diffraction over a slowly varying topography. The time-dependent mild slope equation is written as [4, 1997; p. 254]

$$\frac{\partial^2 \eta}{\partial t^2} - \frac{\partial}{\partial x}\left(cc_g \frac{\partial \eta}{\partial x}\right) - \frac{\partial}{\partial y}\left(cc_g \frac{\partial \eta}{\partial y}\right) + (\sigma^2 - k^2 cc_g)\eta = 0 \tag{1}$$

where η is the free surface displacement, c the wave phase velocity, c_g the wave group velocity, k the wave number, and σ the angular frequency, e.g. $\sigma = 2\pi f = kc$ with f being the wave frequency.

Equation (1) is a second-order hyperbolic equation that has second-order derivatives in both time and space. Few numerical attempts have been made to solve (1) directly, probably due to the seeming difficulty of marching the time step in the second-order time derivative term. As an alternative, for a harmonic wave train, the time derivative term in (1) can be eliminated. This leads to the steady-state mild slope equation [2]:

$$\frac{\partial}{\partial x}\left(cc_g \frac{\partial \eta}{\partial x}\right) + \frac{\partial}{\partial y}\left(cc_g \frac{\partial \eta}{\partial y}\right) + k^2 cc_g \eta = 0 \tag{2}$$

The above equation is of elliptic type and the numerical solution generally requires a significant number of iterations. Berkhoff [2] attempted to solve (2) numerically but the method is restricted to a small domain. Later, Panchang *et al.* [5] adapted a pre-conditional conjugate gradient method to accelerate the convergence rate and thus the model could be applied to a larger area. Li and Anastasiou [6] proposed another solution procedure by using the multigrid technique that also aimed at speeding up the convergence rate.

To avoid the iterative numerical solution for the elliptic Equation (2), one alternative is to parabolize the equation. Radder [7] was the first one to derive the parabolic approximation and applied it to the study of wave passage through a submerged shoal. Dalrymple and Kirby [8] extended the validity range of the parabolic approximation and introduced an angular spectrum concept into their model. Liu [9] summarized the development of parabolic approximation and its application range. It is noted, however, that both Equation (2) and parabolic approximation can only be employed for the steady-state wave solution and thus the transient behaviour of waves cannot be recovered. In reality, the prediction of this transient behaviour may be very important. For example, in a group of wind waves, longer waves travel faster than shorter waves and thus they will arrive at the destination earlier. This phenomenon can only be correctly simulated by solving Equation (1).

The third alternative that retains the transient wave properties is to split the original time-dependent mild slope equation (1) into a pair of first-order hyperbolic equations. The representative study of this approach is by Copeland [10]. An artificial flux term was introduced into the equation and a finite difference form was used to solve the resulting equations. Madsen and Larsen [11] improved the solution procedure by employing an efficient ADI algorithm. Introducing a slow coordinate for the time variable, Li [12] obtained a first-order wave evolution equation with the use of the perturbation method. Recently, Abohadima and Isobe [13] extended Madsen and Larsen's [11] approach to the non-linear wave diffraction computation. The deficiency of such approach is that a pre-step of equation splitting is always needed that introduces the artificial flux and therefore requires the additional effort of solving it. Besides, since there is no definite physical definition for this artificial flux, it imposes uncertainties when the initial and boundary values are specified.

In this study, we shall develop a numerical technique to directly solve the original time-dependent mild slope equation (1). Compared with the previous approaches, this approach is simple, straightforward, and efficient. It can be applied to a large-area computation for transient wave propagation. In the following sections, we will first introduce this new numerical algorithm. The error and stability analyses will be performed to reveal the properties of the new scheme. The numerical model will be first used to simulate the problems of one-dimensional wave propagation in the constant and varying water depth. Comparisons with relevant theories will be made to demonstrate the accuracy of the model. Secondly, numerical simulation will be performed for wave propagation over a submerged shoal on a slope, during which both wave refraction and diffraction are important. Numerical results are compared to available experimental data and other numerical results. Finally, the model is used to study wave transformation around a circular island mounted on a paraboloidal shoal. Waves with different wave periods are simulated and numerical results of wave amplification around the island are compared to existing analytical solutions for the long wave, the short wave, and the wave in intermediate water depth.

NUMERICAL ALGORITHM

Governing equations and boundary conditions

As mentioned earlier, the governing equation we will solve numerically is the time-dependent mild slope equation (1). In this equation, wave number k and angular frequency σ is related by the linear dispersion relationship:

$$\sigma^2 = gk \tanh kh \tag{3}$$

where g is the gravitational acceleration and h is the local still water depth. The phase velocity c and group velocity c_g can be calculated as follows:

$$c = \frac{\sigma}{k}, \quad c_g = \frac{d\sigma}{dk} = \frac{c}{2}\left(1 + \frac{2kh}{\sinh 2kh}\right) \tag{4}$$

There are generally three types of boundaries when Equation (1) is solved, namely, the incoming wave boundary, the radiation (open) boundary, and the solid boundary. The corresponding boundary conditions are summarized below.

At an incoming wave boundary, a linear periodic wave is specified:

$$\eta(t) = \frac{H_0}{2} \sin(\sigma t) \tag{5}$$

where H_0 is the wave height of incident waves. Waves can also be sent at an arbitrary angle.

At a radiation boundary, waves are allowed to leave the domain freely. In this study, we employ the second-order radiation boundary condition derived by Engquist and Majda [14]:

$$\frac{\partial \eta}{\partial t^2} + c\frac{\partial^2 \eta}{\partial n \partial t} - \frac{c^2}{2}\frac{\partial \eta}{\partial s^2} = 0 \tag{6}$$

where n and s represents the normal outward and tangential directions at the radiation boundary. For waves with normal incidence, Equation (6) reduces to the familiar form:

$$\frac{\partial \eta}{\partial t} + c\frac{\partial \eta}{\partial n} = 0 \tag{7}$$

At a solid boundary, full wave reflection is expected and we have

$$\frac{\partial \eta}{\partial n} = 0 \tag{8}$$

Again, n represents the normal direction into the solid surface.

Numerical algorithm

A staggered grid system is used in which all scalar variables (η, k, σ, c, and c_g) are defined at cell centres (Figure 1). The solid area (e.g. a land inside the computational domain) is represented by the shaded cells in Figure 1. The solid boundary condition (8) is applied at the interface between a fluid cell and a solid cell. The arrows in Figure 1 represent the locations where c and c_g are defined in the spatial derivative terms of Equation (1). For simplicity, the numerical algorithm discussed below is based on constant values of Δx, Δy and Δt, though the model can be easily extended to a non-uniform grid system.

With the computational cells and physical variables being such defined, the explicit finite difference scheme for (1) is written as follows:

$$\frac{\eta_{i,j}^{n+1} - 2\eta_{i,j}^{n} + \eta_{i,j}^{n-1}}{(\Delta t)^2} - \frac{(cc_g)_{i+1/2,j}(\eta_{i+1,j}^{n} - \eta_{i,j}^{n})/\Delta x - (cc_g)_{i-1/2,j}(\eta_{i,j}^{n} - \eta_{i-1,j}^{n})/\Delta x}{\Delta x}$$

$$- \frac{(cc_g)_{i,j+1/2}(\eta_{i,j+1}^{n} - \eta_{i,j}^{n})/\Delta y - (cc_g)_{i,j-1/2}(\eta_{i,j}^{n} - \eta_{i,j-1}^{n})/\Delta y}{\Delta y}$$

$$+ [\sigma^2 - k_{i,j}^2 (cc_g)_{i,j}]\eta_{i,j}^{n} = 0 \tag{9}$$

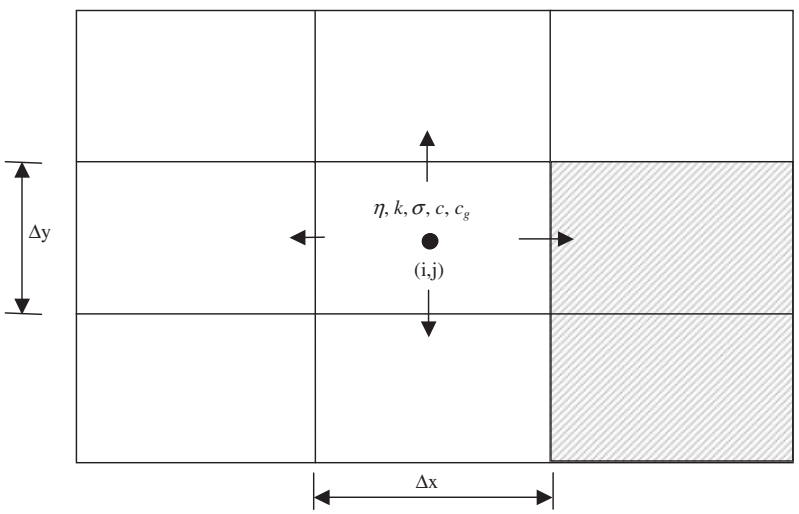

Figure 1. Schematic drawing of computational cells and location definition of physical variables.

The above scheme is similar to the leap-frog method that is often used to solve the system of first-order hyperbolic equations. However, the present method is constructed on three levels of time step for the second-order time derivative term. It is believed that this is the first scheme of this kind proposed for solving the time-dependent mild slope equation. It is noted that σ in (9) is a constant throughout the computation whereas k, c, and c_g are functions of space only. Given a wave period T, the angular frequency can be calculated by $\sigma = 2\pi f = 2\pi/T$. With the topography information of the local still water depth $h(x, y)$, the linear dispersion equation (4) can be employed to find the value of k at every grid point. The corresponding c and c_g will then be calculated by using (4). Re-arranging (9), we have

$$\eta_{i,j}^{n+1} = \eta_{i,j}^{n} + (\eta_{i,j}^{n} - \eta_{i,j}^{n-1}) + \frac{(\Delta t)^2}{(\Delta x)^2}\left[(cc_g)_{i+1/2,j}(\eta_{i+1,j}^{n} - \eta_{i,j}^{n}) - (cc_g)_{i-1/2,j}(\eta_{i,j}^{n} - \eta_{i-1,j}^{n})\right]$$

$$+\frac{(\Delta t)^2}{(\Delta y)^2}\left[(cc_g)_{i,j+1/2}(\eta_{i,j+1}^{n} - \eta_{i,j}^{n}) - (cc_g)_{i,j-1/2}(\eta_{i,j}^{n} - \eta_{i,j-1}^{n})\right]$$

$$+(\Delta t)^2[\sigma^2 - k_{i,j}^2(cc_g)_{i,j}]\eta_{i,j}^{n} = 0 \tag{10}$$

It is noted that when we march the time step from n to $n+1$, the previous time step $(n-1)$ information of η is still needed. In terms of computational effort, this simply means that one more array for the time step $(n-1)$ needs to be stored.

Considering that Equation (1) actually represents an initial-and-boundary-value problem, both the initial and boundary conditions are required. In the computation, we may always start from $n=1$ where there is no wave inside the computational domain (e.g. $\eta(x, y) = 0$ everywhere). Obviously, we can also set $\eta(x, y) = 0$ everywhere at the previous time step $n = 0$. The solution can be then marched forward with the well imposed boundary conditions as defined in (5), (6), and (8).

Truncation errors and stability analysis

A finite difference algorithm always contains numerical errors due to the discretization of a continuous domain into discrete grid points. The characteristics of these numerical errors can be revealed by error analysis based on Taylor expansion. For example, we can expand all terms of η about $\eta_{i,j}^{n}$ as follows,

$$\eta_{i,j}^{n+1} = \eta_{i,j}^{n} + \Delta t\,\frac{\partial \eta_{i,j}^{n}}{\partial t} + \frac{\Delta t^2}{2!}\,\frac{\partial^2 \eta_{i,j}^{n}}{\partial t^2} + \frac{\Delta t^3}{3!}\,\frac{\partial^3 \eta_{i,j}^{n}}{\partial t^3} + \cdots + \frac{\Delta t^m}{m!}\,\frac{\partial^m \eta_{i,j}^{n}}{\partial t^m} + \cdots$$

$$\eta_{i+1,j}^{n} = \eta_{i,j}^{n} + \Delta x\,\frac{\partial \eta_{i,j}^{n}}{\partial x} + \frac{\Delta x^2}{2!}\,\frac{\partial^2 \eta_{i,j}^{n}}{\partial x^2} + \frac{\Delta x^3}{3!}\,\frac{\partial^3 \eta_{i,j}^{n}}{\partial x^3} + \cdots + \frac{\Delta x^m}{m!}\,\frac{\partial^m \eta_{i,j}^{n}}{\partial x^m} + \cdots \tag{11}$$

$$\vdots$$

Substituting (11) into (9) and after some algebraic cancellation, we have

$$\left\{\frac{\partial^2 \eta}{\partial t^2} - \frac{\partial}{\partial x}\left(cc_g\frac{\partial \eta}{\partial x}\right) - \frac{\partial}{\partial y}\left(cc_g\frac{\partial \eta}{\partial y}\right) + (\sigma^2 - k^2 cc_g)\eta\right\}_{i,j}^{n} = \mathrm{TE} \tag{12}$$

The left-hand side of (12) is exactly the same as the left-hand side of (1), the original time-dependent mild slope equation, whereas the right-hand side of (12) will be non-zero in general and it is termed as truncation errors TE. TE is composed of an infinite number of terms and usually we are only concerned with the leading order terms. The expression of TE in (12) is found to be

$$\mathrm{TE} = -\frac{\Delta t^2}{12}\frac{\partial^4 \eta}{\partial t^4} + cc_{\mathrm{g}}\frac{\Delta x^2}{12}\frac{\partial^4 \eta}{\partial x^4} + cc_{\mathrm{g}}\frac{\Delta y^2}{12}\frac{\partial^4 \eta}{\partial y^4} + O(\Delta t^4, \Delta x^4, \Delta y^4) \tag{13}$$

In deriving the above expression, both c and c_{g} have been kept constant to simplify the analysis. The subscripts i, j, and n are also dropped for convenience. We shall easily find that the leading order errors are proportional to squares of Δt, Δx, and Δy and thus the scheme is second-order accurate in both time and space. To better understand the characteristics of TE, we will make a further transformation with the use of (1) to convert the time derivative in (13) to spatial derivatives. The final results are given as follows:

$$\begin{aligned}\mathrm{TE} = {} & \frac{cc_{\mathrm{g}}}{12}(\Delta x^2 - cc_{\mathrm{g}}\Delta t^2)\frac{\partial^4 \eta}{\partial x^4} + \frac{cc_{\mathrm{g}}}{12}(\Delta y^2 - cc_{\mathrm{g}}\Delta t^2)\frac{\partial^4 \eta}{\partial y^4} - \frac{(cc_{\mathrm{g}}\Delta t)^2}{6}\frac{\partial^4 \eta}{\partial x^2 \partial y^2} \\ & + \frac{cc_{\mathrm{g}}\Delta t^2}{6}(\sigma^2 - k^2 cc_{\mathrm{g}})\left(\frac{\partial^2 \eta}{\partial x^2} + \frac{\partial^2 \eta}{\partial y^2}\right) - \frac{\Delta t^2}{12}(\sigma^2 - k^2 cc_{\mathrm{g}})^2 \eta + O(\Delta t^4, \Delta x^4, \Delta y^4)\end{aligned} \tag{14}$$

We can now examine the physical implication of each term in (14). Based on the type of contribution to the second-order time derivative of η on the left-hand side of (12), TE in (14) can be classified into three groups, namely, diffusion (the first three terms), advection (the fourth term), and source (the fifth term). Both advection and source terms are proportional to $\sigma^2 - k^2 cc_{\mathrm{g}}$, which is zero for a long wave, implying that the model will be more accurate in simulating long waves.

There are a few methods for the stability analysis. One of them is von Neumann stability analysis by using Fourier analysis. As an alternative, the Harts Heuristic stability analysis [15], which makes use of the physical contribution of each term in the truncation errors, is employed in this study. Based on the Heuristic stability analysis, the leading diffusion terms could contribute to numerical instability if the numerical diffusivity is negative. This leads us to the establishment of stability condition for this numerical algorithm, i.e. the diffusion coefficients have to be greater than or equal to zero:

$$\Delta x^2 - cc_{\mathrm{g}}\Delta t^2 \geqslant 0 \quad \text{and} \quad \Delta y^2 - cc_{\mathrm{g}}\Delta t^2 \geqslant 0 \;\Rightarrow\; \Delta t \leqslant \min\left(\frac{\Delta x}{\sqrt{cc_{\mathrm{g}}}}, \frac{\Delta y}{\sqrt{cc_{\mathrm{g}}}}\right) \tag{15}$$

In practical computations, Δt calculated from (15) is usually halved as a safety measure.

MODEL VERIFICATION AND DISCUSSION OF RESULTS

In the following paragraphs, we conduct a series of numerical tests to validate the accuracy and efficiency of the model.

Propagation of short and long waves in a constant water depth

In this section, the problem of one-dimensional linear wave propagation in a constant water depth will be studied. There are three objectives in running this numerical test. One is to find the minimum number of grid points required in one wavelength to achieve the acceptable accuracy of numerical results. This will serve as the basis for the later more complicated two-dimensional computation. The second objective is to test the effectiveness of the radiation and solid boundary condition as defined in (6) and (8) for absorbing and reflecting waves. The third objective is to demonstrate the ability of the current model to handle a transient problem, which is important for the real-time wave forecast.

It is well known that the wave energy is transmitted at the speed of group velocity rather than phase velocity. In deep water, the group velocity is always smaller than the phase velocity. Therefore, when a wave train propagates into the calm and deep water, wave crests will vanish at the front end, which moves at a slower speed than the phase velocity. Such effect is clearly demonstrated in Figure 2, in which a short wave train with a wave period of $T = 1\,\mathrm{s}$ is propagated into a calm water with a constant depth of $h = 1\,\mathrm{m}$. The radiation boundary condition (6) is imposed on the right exit. In this case, $c = 1.559\,\mathrm{m/s}$ and $c_g = 0.783\,\mathrm{m/s}$ with $kh = 4.03$. A uniform grid of $\Delta x = 0.10\,\mathrm{m}$ and constant $\Delta t = 0.04\,\mathrm{s}$ are used in the simulation.

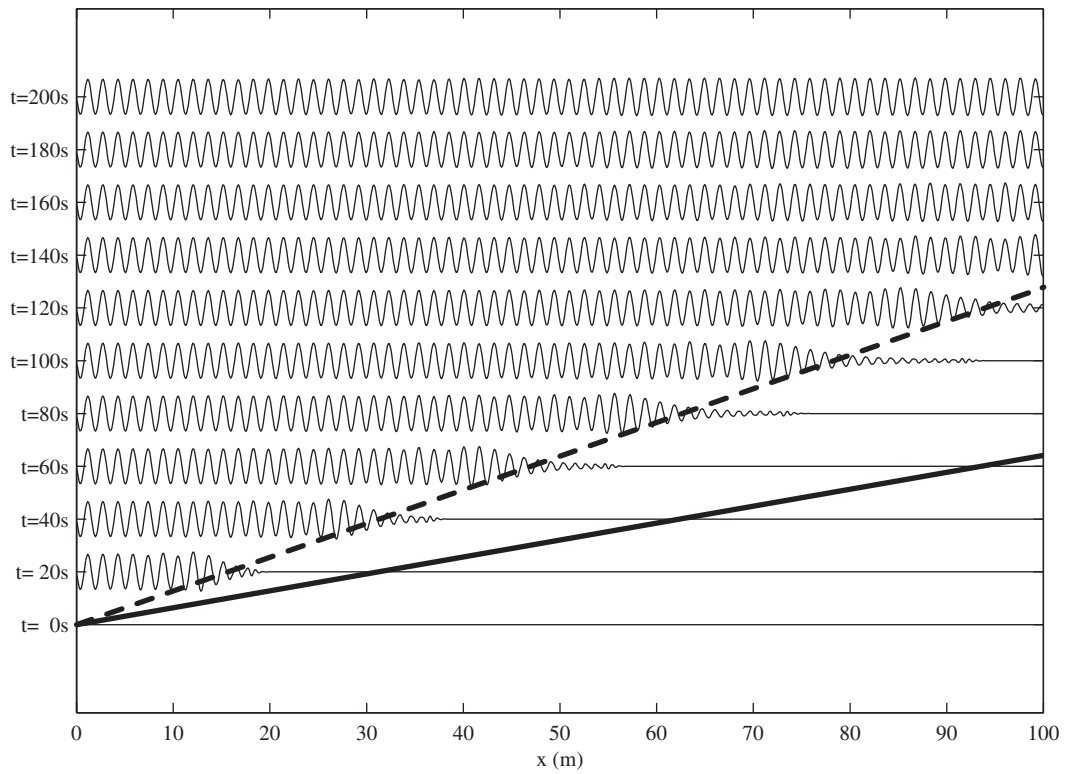

Figure 2. Propagation of short waves ($kh = 4.03$) into calm water; the thick dashed and solid lines represent the front location calculated by c_g and c, respectively.

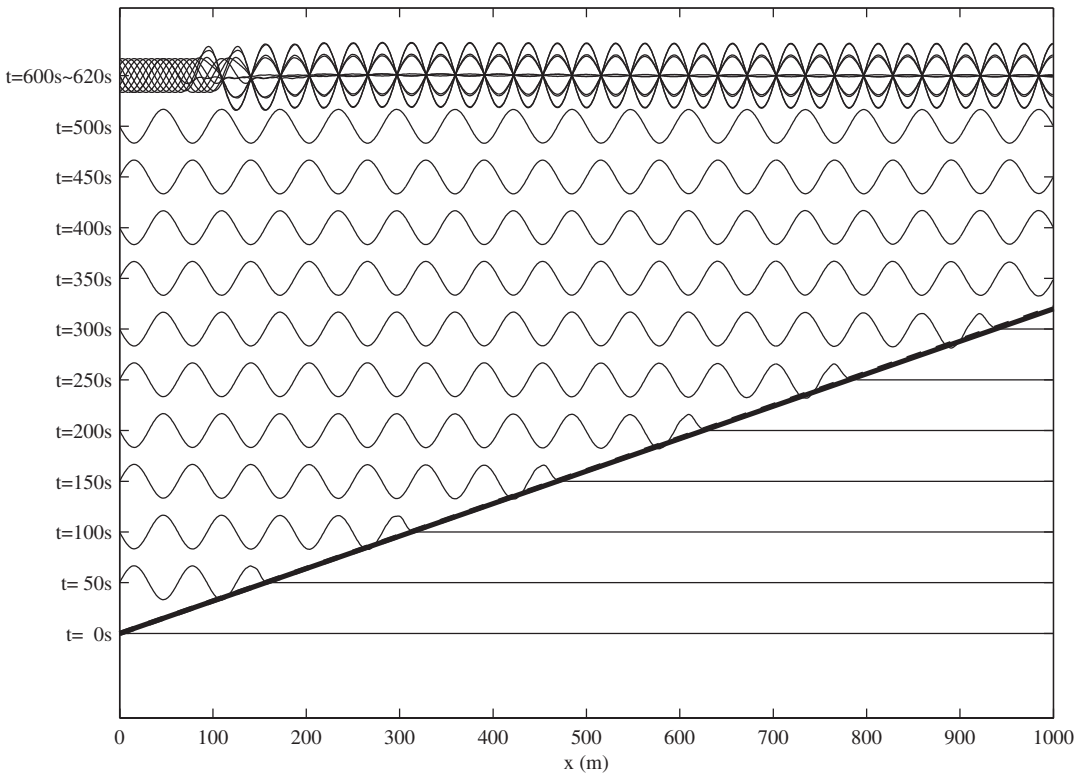

Figure 3. Propagation of long waves ($kh = 0.101$) into calm water; the thick dashed and solid lines (almost identical) represent the front location calculated by c_g and c, respectively; the top curves represent the standing waves when the right boundary changes from the radiation boundary to a solid wall.

Equivalently, one wavelength is covered by about 15 grid points. In Figure 2, we see that the front of the wave train is propagating roughly at the speed of c_g, which is highlighted by the thick dashed line. The thick solid line indicates the front line location calculated by the phase speed c. Some leakage of wave energy across the dashed line is also observed, due to wave dispersion. A well established wave train is observed at $t = 200$ s, when the leading wave front leaves the computational domain freely through the radiation boundary. This demonstrates the effectiveness of the radiation boundary condition as specified in (6). Moreover, it also shows that 15 grid points in one wavelength are adequate to achieve the accurate results.

In the same water depth, a long wave train with a wave period of $T = 20$ s is also simulated. The corresponding values of c and c_g are 3.125 and 3.115 m/s with $kh = 0.101$. A uniform grid of $\Delta x = 1.0$ m and constant $\Delta t = 0.1$ s are used in the simulation. The numerical results are plotted in Figure 3. It is seen that since $c_g \sim c$, the thick dashed line and the thick solid line are almost identical. To further test the solid boundary condition (8), the problem is re-run for a longer time with the right boundary being changed from the radiation boundary to the reflecting solid boundary. The computational results are shown at the top of Figure 3

within one wave period from $t = 600$ to 620 s. It is seen that perfect standing waves are formed in front of the solid wall.

Wave shoaling from deep to shallow water

In this section, we will study a one-dimensional wave shoaling problem, during which we are able to demonstrate the conservation of wave energy in the long distance wave propagation. When waves propagate from the deep to shallow water, the density of wave energy changes with the local group velocity. Accordingly, the wave height, which is proportional to the square root of wave energy density, also changes. The shoaling formula can be easily derived from the conservation of energy flux [16]:

$$c_g E = \text{constant} \Rightarrow c_g H^2 = \text{constant} \tag{16}$$

In the following example, we will simulate an idealized case of a linear wave train propagating across a continental shelf from the deep water to the shallow water. The deep water depth is 3000 m and shallow water depth 40 m, which are connected by a constant slope of $s = 1/50$. The entire computational domain covers 200 km. The incident wave has the wave period of 60 s, a typical value for waves generated during a storm surge. The corresponding values of kh are 3.365 in deep water and 0.213 in shallow water. Therefore, the waves can be regarded as short waves in the deep ocean but long waves in shallow water region. Figure 4 shows the set-up of the problem and the calculated free surface profile. It is observed that the wave height decreases first due to the increase of c_g when waves propagate from deep water to intermediate wave depth. Then the wave height increases rapidly when waves approach to shallow water region. Such feature agrees excellently with the prediction based on the shoaling formula (16). This implies that the model could well conserve wave energy during the long distance wave propagation.

Combined wave refraction and diffraction over a submerged elliptic shoal on a slope

A linear wave train propagating over a submerged elliptic shoal mounted on a slope [17] is a classical problem for verifying a wave refraction–diffraction model. The problem set-up is shown in Figure 5, in which an elliptic shoal is mounted on a sloping beach. The slope-oriented coordinates (x', y') are introduced that is related to the computational co-ordinates (x, y) as follows:

$$x' = (x - x_0)\cos 20^\circ + (y - y_0)\sin 20^\circ, \qquad y' = (y - y_0)\cos 20^\circ + (x - x_0)\sin 20^\circ$$

where (x_0, y_0) is the centre of the shoal. The water depth on the slope is thus:

$$h = \begin{cases} 0.45 - 0.02(5.84 - y') & \text{for } y' < 5.84, \\ 0.45 & \text{for } y' \geqslant 5.84 \end{cases}$$

The water depth above the shoal, e.g. $(x'/4)^2 + (y'/3)^2 < 1$, is modified by

$$h_{\text{shoal}} = h + 0.3 - 0.5\sqrt{1 - \left(\frac{x'}{5}\right)^2 - \left(\frac{y'}{3.75}\right)^2}$$

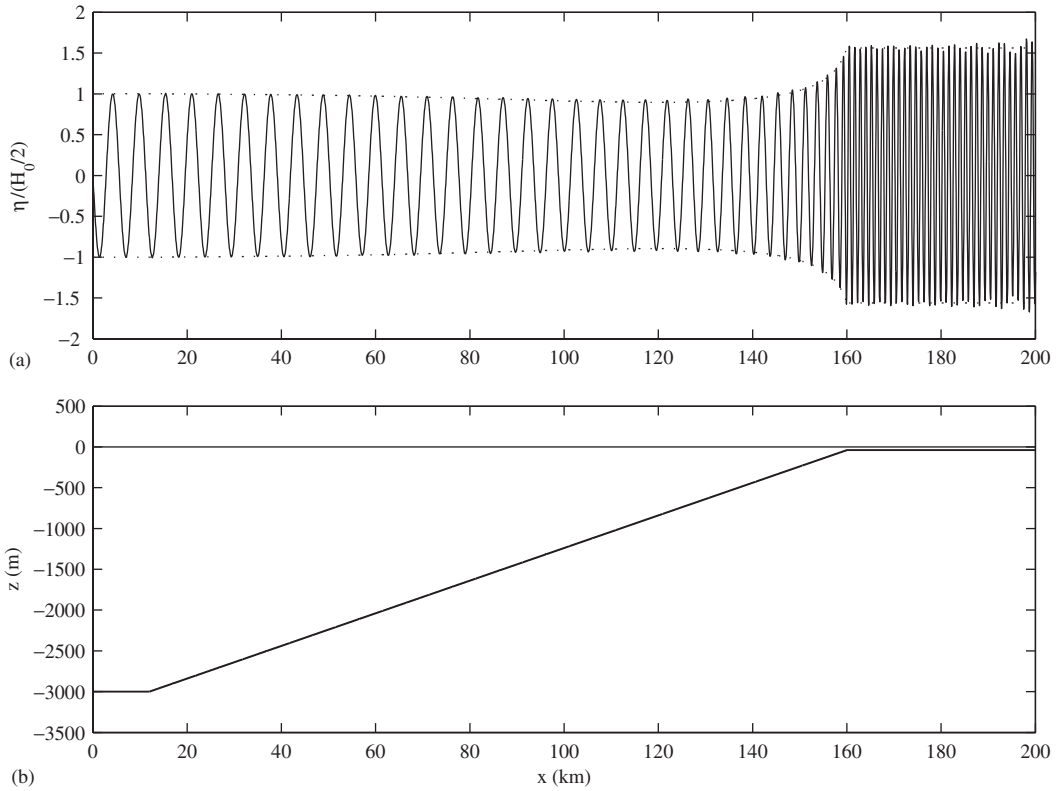

Figure 4. (a) Wave shoaling when propagating from the deep to shallow water depth; the dashed lines represent the envelope predicted by the shoaling formula. (b) Problem set-up.

In this study, the computation domain covers a rectangular region of $-12\,\text{m} \leqslant y \leqslant 25\,\text{m}$ and $-20\,\text{m} \leqslant x \leqslant 20\,\text{m}$. A uniform grid of $\Delta x = \Delta y = 0.1\,\text{m}$ and constant $\Delta t = 0.05\,\text{s}$ is used in the computation. The incident wave has a wave period of $T = 1\,\text{s}$ and the wave height of $H_0 = 0.0464\,\text{m}$. Experimental measurements were made at five sections behind the shoal (i.e. $y = -1, -3, -5, -7,$ and $-9\,\text{m}$)

Numerical computations are carried out up to $t/T = 60$. Totally 20 waves between $t/T = 35$ and $t/T = 55$ are used to calculate the average wave height in the computational domain. The present numerical results are compared with the experimental data and the earlier numerical results by Panchang *et al.* [5] based on the steady mild slope equation (2) (see Figure 6). It is found that the overall agreement between the present results and those by Panchang *et al.* [5] is very good, which is not a surprise. Relatively large discrepancies are found between the numerical results and experimental data at the downstream sections. In fact, these are the common features for the previous numerical modeling based on the linear mild slope equation (e.g. References [5, 6, 17]). The reason for the discrepancies is found to be the non-linear wave effects, which are neglected in the linear wave models. Kirby and Dalrymple [18] proposed a remedy for this problem by using the non-linear dispersion equation instead of the linear equation (4) and they obtained better results in their parabolic approximation solution.

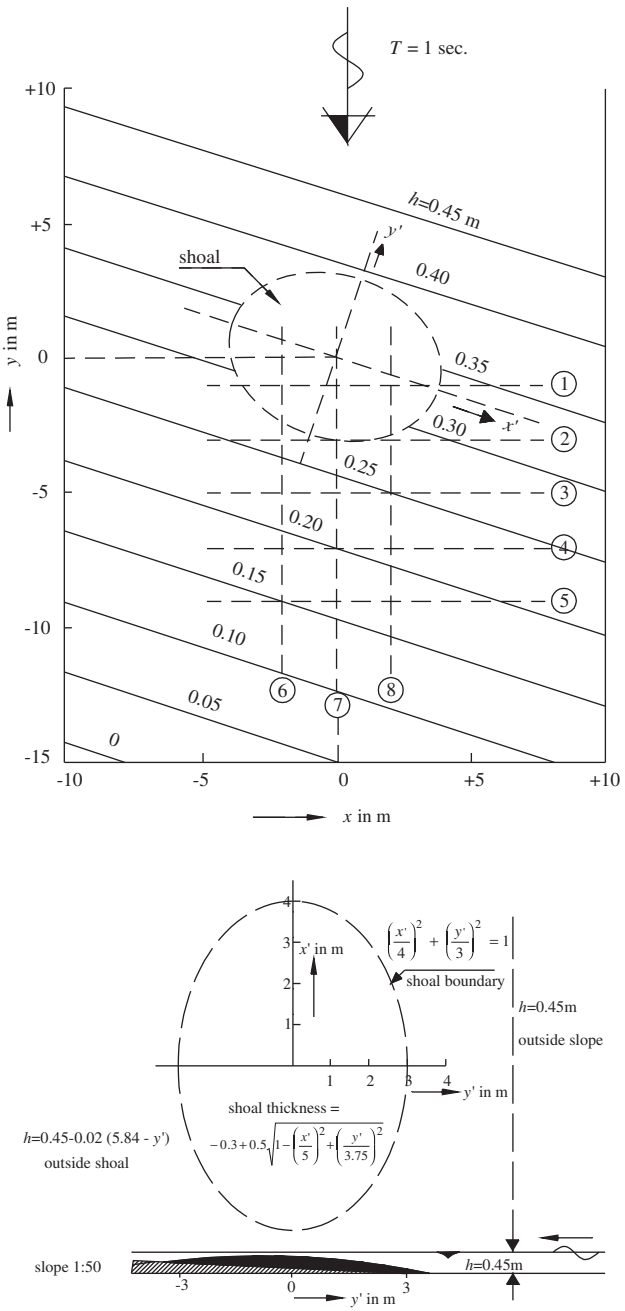

Figure 5. Problem set-up in Berkhoff *et al.*'s [17] study.

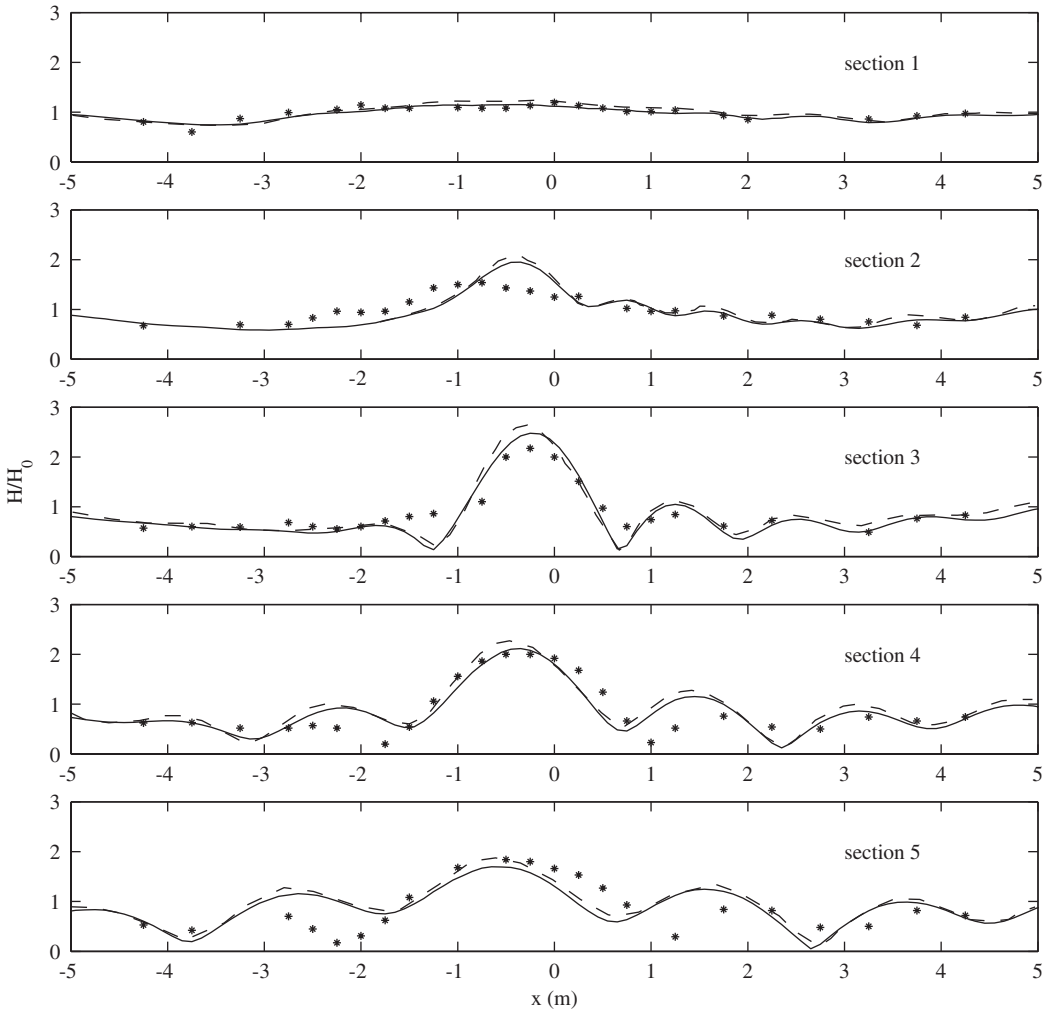

Figure 6. Comparisons of wave amplification among the present numerical results (solid lines), numerical result for the steady mild slope equation by Panchang *et al.* [5] (dashed line), and experimental data (asterisks) at five sections behind the shoal.

Panchang *et al.* [5] confirmed this finding when they applied the same non-linear equation into their elliptic mild slope equation model. Li and Fleming [19] solved a fully non-linear wave model and found that with the inclusion of non-linear effects, better results were indeed achieved. It is one of our future aims to extend the current model so that it can include the non-linear effects.

Maximum wave runup around a cylindrical island mounted on a paraboloidal shoal

Storm surges can cause severe coastal flooding and have been reported to claim both the loss of life and the damage of property (e.g. References [20, 21]). In general, the coastal flooding is caused by the rise of mean water level due to the large-scale atmospheric pressure

variation, which is enhanced by the attack of waves induced by strong winds. Conventionally, the mean water level is simulated by the depth-integral equation models and the waves by the energy spectrum models (e.g. WAM by WAMDI Group [22] and SWAN by Booij *et al.* [23]). Recently, the coupling of two types of models was implemented by Mastenbroek *et al.* [24]), Zhang and Li [25], and McInnes *et al.* [26]. In this study we shall be only concerned about the wave modelling part. Although the energy spectrum models have the advantage of simulating large-scale variation of wave height, they lack of ability to calculate wave diffraction. Only limited progresses were made in recent years to resolve this problem (e.g. [27]). In reality, wave diffraction can be very important. For example, the largest wave runup can sometimes occur on the lee side rather than the front side of the island due to the combined wave refraction and diffraction (e.g. [28]). In order to predict accurately the coastal flooding, the numerical model based on the mild slope equation as developed in this study could become an alternative to the energy spectrum models to predict wave propagation up to certain distance away from the shoreline where the linear wave assumption is still valid.

In this section, we will calculate the maximum wave runup around an idealized cylindrical island mounted on a paraboloidal shoal [29], for which various analytical solutions are available for model verification. The cylindrical island has a radius of $r_0 = 10\,000\,\text{m}$ and the geometry of the paraboloidal shoal can be described by a function of $h = \alpha r^2$ where $\alpha = 4/900\,000$ (all lengths are in meters; see Figure 7). When a wave train propagates towards the island, it experiences a combined effect of wave shoaling, refraction, diffraction, and reflection. This imposes a great challenge for a numerical model and it is our task here to check whether the present model can still generate reliable results.

Waves with different periods from $T = 720,\ 120$ to 24 s are to be simulated. The wave amplification factors along the shoreline of the island are calculated, which can be used to predict the potential risk of coastal flooding. Firstly, consider the case of $T = 720\,\text{s}$, which falls into the lower range of seismic waves (e.g. tsunami) or the upper range of waves generated during a storm. In this case, waves can be regarded as long wave even in the deep water region of $h = 4000\,\text{m}$ where $kh = 0.177$. The value of kh reduces to 0.058 in shallow water region at the shoreline. Therefore, the analytical solution derived from the linear shallow water equation, which is the asymptotic form of the mild slope equation for very long waves, can accurately predict wave amplification factors along the island [29]. In this case, since the wavelength is much larger than the island, the numerical accuracy depends on the resolution of the island. We have used a uniform grid of $\Delta x = \Delta y = 100\,\text{m}$, from which 100×100 grid points are employed to resolve the island configuration. The entire computation is chosen to be $200\,\text{km} \times 200\,\text{km}$ and is resolved by a 2000×2000 grid system. A constant $\Delta t = 0.25\,\text{s}$ is used. In total 16 000 time steps have been carried out that correspond to a total time of 4000 s. Figure 8 shows the comparisons of wave amplification between numerical results from the current model and analytical solution by Homma [29]. The overall agreement is excellent, except for a small underestimation of wave height on the front side of the island (e.g. $\theta = 180^\circ$). It is found that for this type of wave incidence, the maximum wave runup occurs on the front of the island right facing the wave attack. On the lee side, the wave amplitude is only about half of that on the front.

The next case we investigate has the wave period of $T = 120\,\text{s}$. The values of kh in deep and shallow water are 1.299 and 0.357, indicating that waves start from intermediate depth and become shallow water waves near the island. Such case cannot be accurately predicted by Homma's [29] theory which is only valid for the shallow water depth. Recently, an analytical

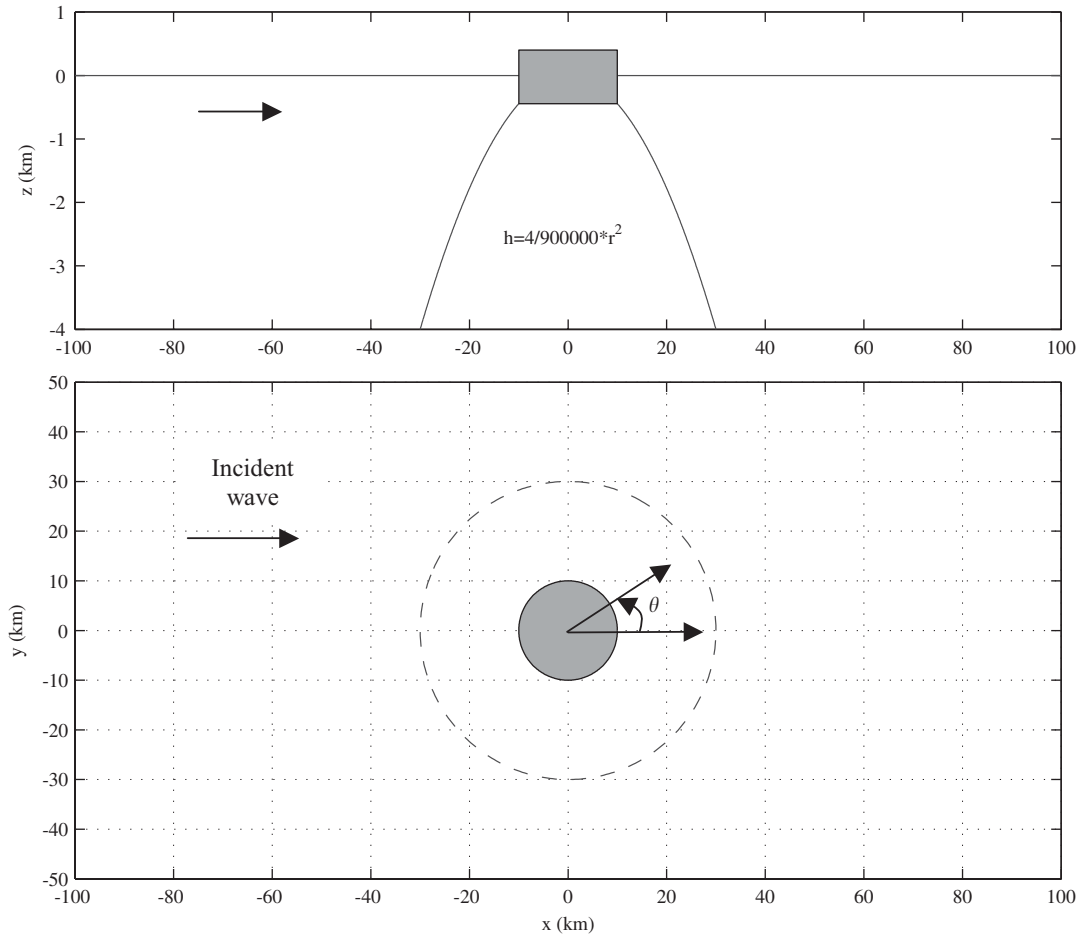

Figure 7. Set-up of Homma's island; $\theta = 0^\circ$ is aligned with x-axis.

solution based on the elliptic mild slope equation with an approximate dispersion relationship was proposed by Liu *et al.* [30]. The solution has proved to be consistently accurate for predicting wave amplification in deep, intermediate, and shallow water. We shall use this theory to validate our numerical results. In the numerical simulation, the same mesh system as used in the case of $T = 720$ s is adapted. Comparisons are given in Figure 9 and very good agreement is again obtained. Compared with the case of $T = 720$ s, more oscillations are observed along the island in Figure 9. An interesting finding is that the wave amplification factor reaches about 4 on the lee side of the island (e.g. $\theta = 0^\circ$), whereas it is only about 2 on the front side. This indicates a strong energy focusing and trapping by the island due to the combined wave refraction and diffraction. Under such circumstance, the lee side of island is still exposed to the severe risk of coastal flooding.

The last case we will examine has $T = 24$ s. This wave period is within the lowest range of storm waves. In this case, the values of kh in deep and shallow water are 27.9753 and 3.1201,

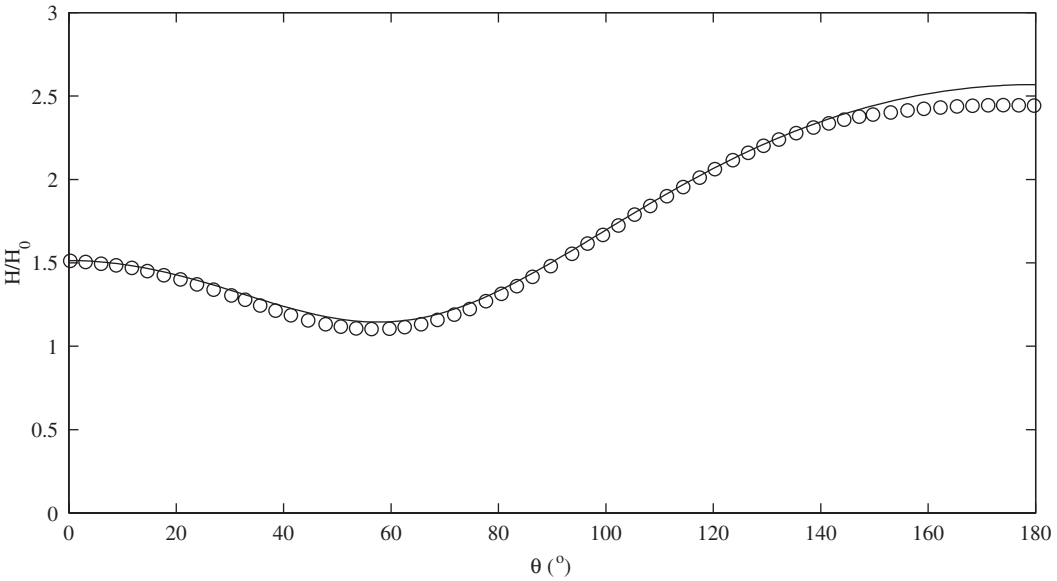

Figure 8. Comparisons of wave amplification along the shoreline of the island between the numerical results (circle) and the analytical solution by Homma [29] (line) for $T = 720$ s.

respectively. This means that the waves can be classified as short waves in the entire domain. In other words, the variation of bottom topography has little influence on the final results. Therefore, the analytical solution derived by MacCamy and Fuchs [31] based on Helmholtz equation for the wave diffraction around a large circular cylinder is a good reference to validate our numerical results. In this case, the wavelength is only about 900 m and thus our previous mesh discretization with $\Delta x = \Delta y = 100$ m is not enough to resolve wave motion. In order to gain adequate resolution, we first reduce the computation domain to 100 km $\times$ 100 km with the mesh size of $\Delta x = \Delta y = 50$ m. The calculated wave amplification is compared to the analytical solution in Figure 10. It is seen that the model captures the general trend of the variation of wave amplitude along the shoreline, though fluctuations are found in the numerical results. These fluctuations are caused by the discretization of smooth shoreline into stair-type of solid boundary as illustrated in Figure 1. The magnitude of these fluctuations should be reduced by further refining the mesh size, which is confirmed by running the same problem with a smaller mesh size of $\Delta x = \Delta y = 25$ m. The agreement with the analytical solution is greatly improved as shown in Figure 10.

Finally, we will roughly estimate the computational resource required for a practical simulation. All the above simulations have been performed on a PC (Pentium IV 1.8 GHz) with the memory of 512 MB. With such configuration, we are able to run a mesh system up to 3000×3000. The CPU time is about 72 h for carrying out a computation up to 15 000 time steps, which in most of cases are sufficient for one run. If we use 20 grid points to resolve one wavelength, we are able to cover a range of 150×150 waves, an area much bigger than what most of the previous phase-resolving numerical models can afford. Considering a wave period of $T = 60$ s, a typical value for waves generated during a storm, the wavelength in the shallow water of $h = 444$ m is about 3600 m. The affordable computational domain is then

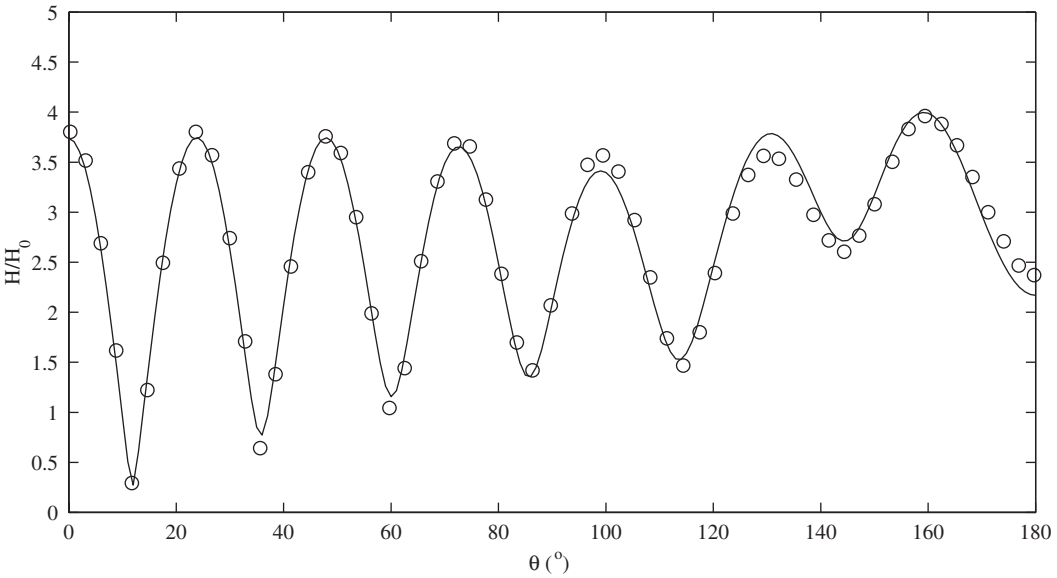

Figure 9. Comparisons of wave amplification along the shoreline of the island between the numerical results (circle) and the analytical solution by Liu *et al.* [30] (line) for $T = 120$ s.

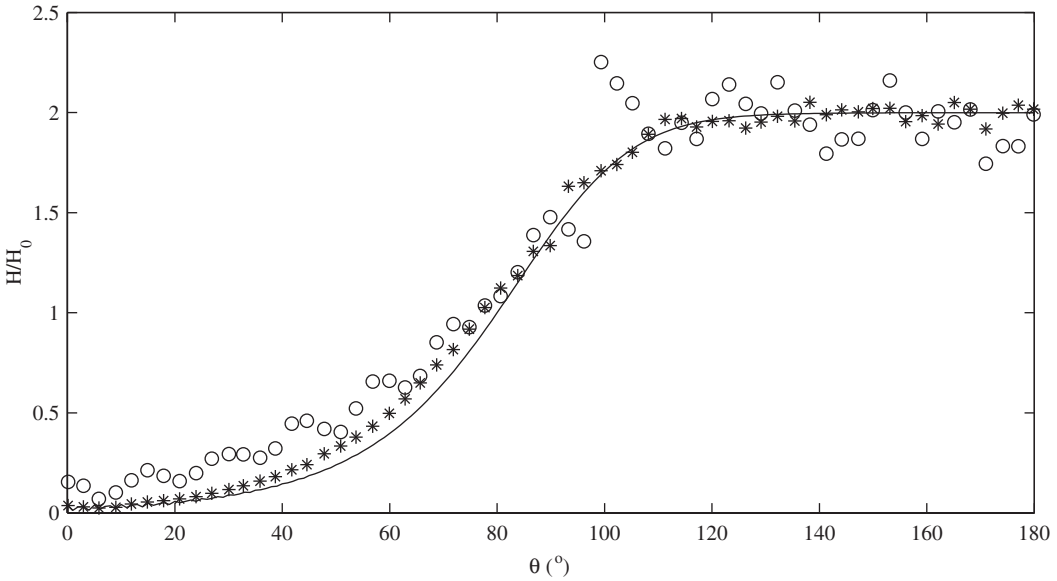

Figure 10. Comparisons of wave amplification along the shoreline of the island between the numerical results (circle: $\Delta x = \Delta y = 50$ m; asterisk: $\Delta x = \Delta y = 25$ m) and the analytical solution by MacCamy and Fuchs [31] (line) for $T = 24$ s.

equivalent to 540 km × 540 km. This computational domain can be doubled or even tripled with the code parallelization possible in the near future.

CONCLUSION

In this study, a new numerical algorithm has been developed to solve the time-dependent mild slope equation, which has a second-order hyperbolic form. The algorithm has a compact form and is second-order accurate in both time and space. The algorithm has the similar structure to the leap-frog method but is constructed on three levels of time step for the second-order time derivative term. Numerical analyses show that the leading truncation errors are composed of diffusion, advection, and source terms, the latter two of which will vanish for long waves. The numerical scheme is conditionally stable with the criterion of $\Delta t \leqslant \min(\Delta x, \Delta y)/\sqrt{cc_g}$.

The numerical model has been verified for one- and two-dimensional problems. For one-dimensional problems, the propagating of short and long waves in a constant water depth is first studied and it is demonstrated that the model can accurately capture the transient feature of wave advancement into the calm water, during which the crests vanish in the front end of wave train for short waves. This is an important feature for real-time wave forecast, which requires the correct prediction of the arrival time of the wave front. Waves propagating over an idealized continental shelf are also studied and the numerical results of wave amplitude perfectly match the shoaling formula, showing the satisfactory characteristics of energy conservation of the present algorithm.

For two-dimensional verification, wave focusing behind a submerged elliptic shoal mounted on a slope [17] is studied. The present numerical results are compared with the experimental data and other numerical results at five cross-sections behind the shoal. Reasonable agreements are obtained. Some discrepancies from the experimental data are observed at the downstream sections, mainly due to the non-linear effects that have not been included in the present linear model. It is one of the future objectives to extend the present algorithm to a non-linear mild slope equation so that the application range of the model will be widened.

Finally, we have studied the case of wave runup around a cylindrical island mounted on a paraboloidal shoal [29]. In this case, the combined effects of wave shoaling, refraction, diffraction, and reflection are present and they impose a great challenge to the numerical modelling. Waves with different wave periods, e.g. $T = 720,\ 120$, and 24 s are simulated. These waves represent long, intermediate, and short waves, respectively, and cover a typical range of waves generated during a storm. The numerical results are compared with the available analytical solutions derived from the linear shallow water equation [29], the mild slope equation with an approximate dispersion relation [30], and Helmholtz equation [31]. The overall comparisons are excellent.

ACKNOWLEDGEMENTS

The research work herein was supported, in part, by the research grants from National University of Singapore (R-264-000-121-112) and Meteorological Service Singapore (R-264-000-121-291).

REFERENCES

1. Eckart C. The propagation of gravity waves from deep to shallow water. *Circular 20*, *National Bureau of Standards* 1952; 165–173.

2. Berkhoff JCW. Computation of combined refraction diffraction. *Proceedings of the 13th International Coastal Engineering Conference*. ASCE: New York, 1972; 471–490.
3. Kirby JT. A note on linear surface wave-current interaction over slowly varying topography. *Journal of Geophysical Research* 1984; **89**(C1):745–747.
4. Dingemans MW. *Water Wave Propagation over Uneven Bottoms. Advanced Series on Ocean Engineering*, vol. 13. World Scientific: Singapore, 1997.
5. Panchang VG, Pearce BR, Wei G, Cushman-Roisin B. Solution of the mild slope wave problem by iteration. *Applied Ocean Research* 1991; **13**(4):187–199.
6. Li B, Anastasiou K. Efficient elliptic solver for the mild-slope equation using the multigrid technique. *Coastal Engineering* 1992; **16**:245–266.
7. Radder AC. On the parabolic equation method for water-wave propagation. *Journal of Fluid Mechanics* 1979; **95**(1):159–176.
8. Dalrymple RA, Kirby JT. Models for very wide-angle water waves and wave diffraction. *Journal of Fluid Mechanics* 1988; **192**:33–50.
9. Liu PL-F. Wave transformation. In *The Sea*, *Ocean Engineering Science*, vol. 9A., Lemehaute B (ed.). Wiley: New York, 1990; 27–63.
10. Copeland GJM. A practical alternative to the "mild-slope" wave equation. *Coastal Engineering* 1985; **9**:125–149.
11. Madsen PA, Larsen J. An efficient finite-difference approach to the mild-slope equation. *Coastal Engineering* 1987; **11**:329–351.
12. Li B. An evolution equation for water waves. *Coastal Engineering* 1994; **23**:227–242.
13. Abohadima S, Isobe M. Linear and nonlinear wave diffraction using the nonlinear time-dependent mild slope equations. *Coastal Engineering* 1999; **37**:175–192.
14. Engquist B, Majda A. Absorbing boundary conditions for the numerical simulation of waves. *Mathematics of Computation* 1977; **31**(139):629–651.
15. Roache PJ. *Fundamentals of Computational Fluid Dynamics*. Hermosa Publisher, New Mexico, USA, 1998.
16. Dean RG, Dalrymple RA. *Water Wave Mechanics for Engineers and Scientists. Advanced Series on Ocean Engineering*, vol. 2. World Scientific: Singapore, 1991.
17. Berkhoff JCW, Booy N, Radder AC. Verification of numerical wave propagation models for simple harmonic linear water waves. *Coastal Engineering* 1982; **6**:255–279.
18. Kirby JT, Dalrymple R. Verification of a parabolic equation for propagation of weakly-nonlinear waves. *Coastal Engineering* 1984; **8**:219–232.
19. Li B, Fleming CA. A three dimensional multigrid model for fully nonlinear water waves. *Coastal Engineering* 1997; **30**:235–258.
20. Blier W, Keefe S, Shaffer WA, Kim SC. Storm surges in the region of western Alaska. *Monthly Weather Review* 1997; **125**(12):3094–3108.
21. Rappaport EN. Loss of life in the United States associated with recent Atlantic tropical cyclones. *Bulletin of the American Meteorological Society* 2000; **81**(9):2065–2073.
22. WAMDI Group. The WAM model—a third generation ocean wave prediction model. *Journal of Physics Oceanography* 1988; **18**:1775–1810.
23. Booij N, Ris RC, Holthuijsen LH. A third-generation wave model for coastal regions: 1. Model description and validation. *Journal of Geophysical Research* 1999; **104**(C4):7649–7666.
24. Mastenbroek C, Burgers G, Janssen PAEM. The dynamical coupling of a wave model and a storm surge model through the atmospheric boundary layer. *Journal of Physical Oceanography* 1993; **23**:1856–1866.
25. Zhang MY, Li YS. The synchronous coupling of a third-generation wave model and a two-dimensional storm surge model. *Ocean Engineering* 1996; **23**(6):533–343.
26. McInnes KL, Hubbert GD, Abbs DJ, Oliver SE. A numerical modelling study of coastal flooding. *Meteorology and Atmospheric Physics* 2002; **80**:217–233.
27. Booij N, Holthuijsen LH, Doorn N, Kieftenburg ATMM. Diffraction in a spectral wave model. *Proceedings of the 3rd International Symposium on Ocean Wave Measurement and Analysis*, *WAVES'97*. ASCE: New York, 1997; 243–255.
28. Liu PL-F, Cho YS, Briggs MJ, Lu UK, Synolakis CE. Runup of solitary waves on a circular island. *Journal of Fluid Mechanics* 1995; **302**:259–285.
29. Homma S. On the behavior of seismic sea waves around circular island. *Geophysical Magazine* 1950; **21**: 199–208.
30. Liu HW, Lin PZ, Shankar NJ. A power series solution of the mild-slope equation for waves around a circular island mounted on a paraboloidal shoal. *Coastal Engineering* 2004, under review.
31. MacCamy RC, Fuchs RA. Wave forces on piles: a diffraction theory. *Technical Memorandum*, vol. 69, US Army Corps of Engineering, Beach Erosion Board, Washington, DC, 1954.

